Defence Technology 17 (2021) 1852–1863

Contents lists available at ScienceDirect

Defence Technology

journal homepage: www.keaipublishing.com/en/journals/defence-technology

Field test and probabilistic analysis of irregular steel debris casualty risks from a person-borne improvised explosive device

Piotr W. Sielicki [a, *], Mark G. Stewart [c], Tomasz Gajewski [a], Michał Malendowski [a], Piotr Peksa [a], Hasan Al-Rifaie [a], Robert Studziński [b], Wojciech Sumelka [a]

[a] Institute of Structural Analysis, Faculty of Civil and Transport Engineering, Poznan University of Technology, 5 Maria Skłodowska-Curie Square, 60-965, Poznan, Poland
[b] Institute of Building Engineering, Faculty of Civil and Transport Engineering, Poznan University of Technology, 5 Maria Skłodowska-Curie Square, 60-965, Poznan, Poland
[c] Centre for Infrastructure Performance and Reliability, The University of Newcastle, University Drive, Callaghan, NSW, 2308, Australia

ARTICLE INFO

Article history:
Received 31 August 2020
Received in revised form
12 October 2020
Accepted 28 October 2020
Available online 24 November 2020

Keywords:
Flying fragments
Human safety
Person-borne improvised explosive device experiment
Probabilistic analysis

ABSTRACT

Person-borne improvised explosive devices (PBIEDs) are often used in terrorist attacks in Western countries. This study aims to predict the trajectories of PBIED fragments and the subsequent safety risks for people exposed to this hazard. An explosive field test with a typical PBIED composed of a plastic explosive charge and steel nut enhancements was performed to record initial fragment behaviour, including positions, velocity, and trajectory angles. These data were used to predict the full trajectory of PBIED fragments using a probabilistic analysis. In the probabilistic analyses a probability of fatality or serious injury was computed. Based on the results presented, many practical conclusions can be drawn, for instance, regarding safe evacuation distances if a person were exposed to a suspected PBIED.

1. Introduction

Improvised explosive devices (IEDs) have been a weapon of choice for terrorist attacks in Europe, North America, and other Western countries. Recent IED attacks include trains in Madrid (2004); trains and a bus in London (2004); government buildings in Oslo (2011), Stade de France, the Bataclan Theatre, and a café in Paris (2015); an airport and train station in Brussels (2016), and Manchester Arena (2017). Most of these IED attacks involved a person-borne improvised explosive device (PBIED) containing less than 10 kg of explosives [1]. This conclusion is not unexpected; an analysis of bomb incidents over the past 15 years found that most IEDs weigh less than 5 kg [2]. Most of the attacks were conducted in urban environments where structures are exposed to the blast effects. As a result, there has been substantial research into the structural damage to buildings, bridges, pipelines, trains, and other infrastructure elements from blast pressure and impulse [3,4]. However, most terrorist attack casualties in Western countries (post-9/11) have been from primary and secondary injuries [5,6] due to fragmentation and blast overpressure (e.g. lung rupture, brain acceleration, whole-body displacement, or skull fracture) rather than from falling columns, beams, slabs, or other structural components [7,8]. Infrastructure structural components have proven highly resilient to terrorist IED attacks; however, more research is needed to understand casualty risks from bomb fragmentation and blast overpressure hazards, especially from PBIEDs. Understanding of initial fragment mass, velocity, and distribution as well as the fragments' drag coefficients, kinetic energy, throw range, and density probabilities is essential. For example, fragment mass, count distributions, and velocities are used in SAFER (Safety Assessment for Explosives Risk) and VAPO (Vulnerability Assessment and Protection Option), software developed by the U.S. Department of Defense Explosive Safety Board (DDESB) and the Defense Threat Reduction Agency (DTRA) to predict fragmentation distributions and casualty risks. However, these software programs are best suited to assessing military ordnance safety risks because they utilise predefined munitions parameters and fragment masses that are not easily applied to IEDs. IED fragment density is highly spatial, not symmetric, and heavily reliant on the explosive's

* Corresponding author.
E-mail address: piotr.sielicki@put.edu.pl (P.W. Sielicki).
Peer review under responsibility of China Ordnance Society

https://doi.org/10.1016/j.dt.2020.10.009

placement and the source material of the fragments. This paper was prompted by Yokohama et al.'s [9] conclusions where they noted that, "IED fragmentation data is unavailable since it is not published in the open literature; " "IED fragmentation is difficult to predict for its stochastic nature; " and "the current modelling capability of the IED fragmentation is less mature." There are significant uncertainties and variabilities associated with modelling primary fragmentation. The explosive safety distances proposed by the U.S. Department of Defense Explosive Safety Board [10] consider some of these uncertainties when predicting casualty risks from accidental detonation of military ordnances. The DDESB [10] suggests that, when predicting casualty risks from accidental detonation of military ordnances, model accuracy is low at between −95% and +200%. Clearly, there is a need for improved modelling and statistical characterisation of the main variables associated with fragmentation. Characterisation of IED blast and fragmentation uncertainties using stochastic (probabilistic) methods is a logical step to improve risk estimates.

One of the most common PBIEDs worldwide is the suicide vest. These devices were used in the 2015 Paris attacks and contained no more than 10 kg of triacetone triperoxide (TATP) as the explosive agent. Pachman et al. [11] examined TATP and found an average TNT equivalent from incident overpressure equal to 70%, and for impulse of the positive phase of the blast wave, it reduces to 55%; it may be assumed that a similar effect would be obtained from an approximately 6–8 kg TNT charge. Thus, an explosive charge of modest mass may significantly accelerate IED fragments, increasing the risk of mass casualties.

The present paper assesses the casualty risks and safe evacuation distances for people exposed to suicide vest PBIEDs. The main aim of this paper is an improved understanding of the primary fragmentation of PBIED vests containing hundreds of steel nuts; its secondary aim is for the knowledge gained herein to be generalisable to other improvised projectiles intended to result in mass casualties.

2. Materials and methods

2.1. Experiment setup

The primary objective of this experiment was to measure the initial velocity, trajectory angle, final range, and kinetic energy of fragments from a PBIED. Due to security reasons, it is not possible to show all details of the assembly and detonation of a PBIED. Nevertheless, the concept and geometry presented herein may be viewed as representative of some PBIEDs used in the 2015 November attacks in Paris. In this study, 4.43 g M8 stainless steel hex nuts were used as enhancements. Hex nuts were chosen for representing the flying projectiles because they are one of the most used in PBIED; mainly because they are easy to get by trade without raising suspicions. The setup of the device was built on the experiences of special forces, which often investigates such explosive devices. Thus, hex nuts arrangement and quantity are close to the real-world cases. The nuts were layered in front of the explosive charge in an open-faced sandwich, as shown in Fig. 1. The layer of nuts comprised nine rows and 24 columns (a total of 216 nuts in one layer) measuring 120 mm × 310 mm, see Fig. 1(b). The PBIED—shown at A in Fig. 2(a)—consisted of the suicide vest containing charge of plastic explosive number four (PE4), a similarly-sized layer of clay a few centimetres thick, a rigid, bullet-proof layer of Kevlar, and the layer of 216 hex nut projectiles weighing a total of 957 g. The PBIED was fixed to wooden stakes at a height of 0.9 m above the ground level, as shown in Fig. 2(b). Due to the sensitivity of the data the mass of the IED was classified.

The full experimental site is shown in Fig. 3. One of the objectives of this paper is to assess the trajectory of the debris originating from the PBIED; another objective is to evaluate the effect of PBIED fragment distribution on the car, shown at D in Figs. 3 and 4. Fragment distribution on the plywood panels (B, C, and E) remains a topic for future research. Plywood panel B is situated perpendicular to the camera view in order to create the background for camera for observing horizontally flying nuts. The car, D, is located 10.8 m from the PBIED, see Figs. 2(a) and Fig. 3.

An important aspect of this test was to measure the velocity and trajectory of the hex nut enhancements during the first 10 ms of flight after acceleration by the explosive charge. Fragment velocity data was collected through video recording and later post-

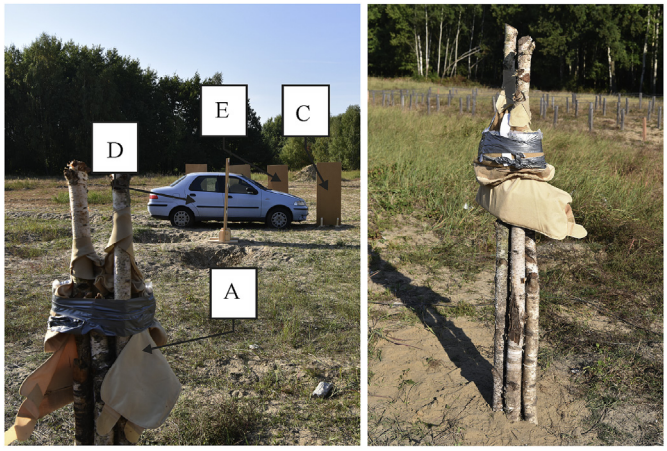

Fig. 2. PBIED experiment set up: (a) back view and (b) front view.

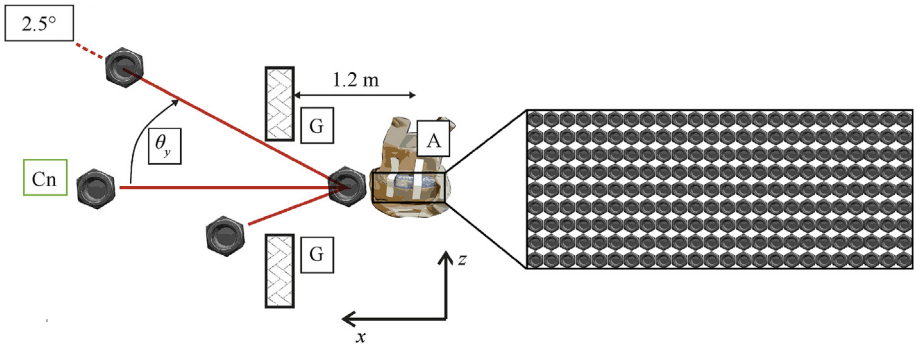

Fig. 1. Elements of the PBEID used in the experiments: (a) the set-up plan and (b) the layer of 216 hex nuts.

Fig. 3. Full (side) view of the experiment site.

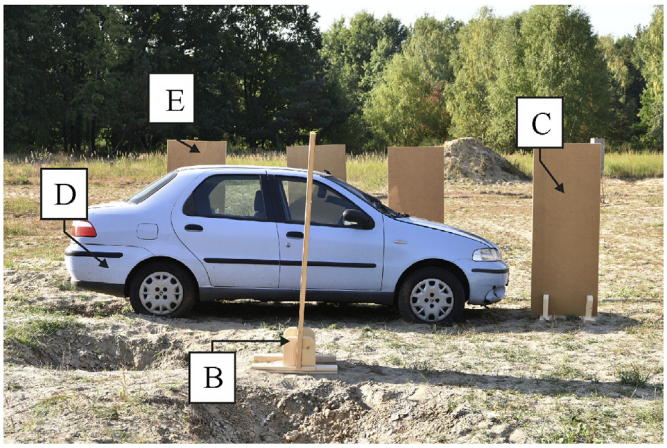

Fig. 4. Small-size car used in the experiment.

processing of the data. The magnitude of velocity was estimated for 74 fragments using a high-speed video in combination with velocity screens and witness screens.

2.2. Fragment loading measurements

Several factors influence the reliability of the measurements of highly dynamic experiments. Verification that the values recorded are physically correct was allowed for in test preparations. Based on the previous experiences of the Poznan research group, it was crucial to define the location of the high-speed camera to obtain an accurate measurement of velocity of objects that could be traveling faster than the speed of sound. The goal was to measure 10 to 20 individual nuts, each with a different velocity, flying at different horizontal and vertical angles.

The test scheme is presented in Fig. 5. It was assumed that the projectiles would be launched at point A and fly to Cn. The high-speed camera recording system was capable of following the objects in their first 10 m of the flight—from the detonation position, A, to the car, D. This trajectory is presented in Fig. 5, see red (rising) and green (falling) curves.

Another important description of the trajectory of each nut is the vertical angle between the trajectory and horizontal direction—the angle θ_x in Fig. 5. The perfect measurement assumes that a separated nut followed by the measurement equipment can be found at the final X_{MAX} distance, Cn. The objective of this paper is to predict the trajectory of all nuts during full flight trajectory using only initial launch conditions. This prediction can be obtained based on a classical system of equations of motion:

$$\begin{cases} \dfrac{d^2x}{dt^2} = -\dfrac{C_{dx}A_x\rho}{2m}\left(\left(\dfrac{dx}{dt}\right)^2 + \left(\dfrac{dy}{dt}\right)^2\right)^{\frac{1}{2}}\dfrac{dx}{dt} \\ \dfrac{d^2y}{dt^2} = -\dfrac{g}{m} - \dfrac{C_{dy}A_y\rho}{2m}\left(\left(\dfrac{dx}{dt}\right)^2 + \left(\dfrac{dy}{dt}\right)^2\right)^{\frac{1}{2}}\dfrac{dy}{dt} \end{cases} \quad (1)$$

where x and y are the coordinates of the plane of interest; t is time; C_{dx} and C_{dy} are the drag coefficients in x and y directions, respectively; A_x and A_y are the nut area projections in x and y directions, respectively; ρ is air density; g is gravity; and m is fragment mass. The drag coefficients C_{dx} and C_{dy} were assumed at 0.8 for horizontal and 1.5 for vertical ascending and descending movements. For further consideration of the trajectory assessment, the cross-sectional areas (A_x, A_y) of the nut are necessary. Because of the uniform geometry of projectiles, the authors assumed that the projected areas would be measured in two major orientations. Hence, the vertical and horizontal cross-sectional areas of a nut were equal $A_x = 105.5$ mm^2 and $A_y = 129.3$ mm^2, respectively. In general, the shapes of projectiles may be highly irregular and thus, determining its drag coefficients and projected areas may be difficult to estimate, see Moxnes et al. [12] and Kljuno and Catovic [13].

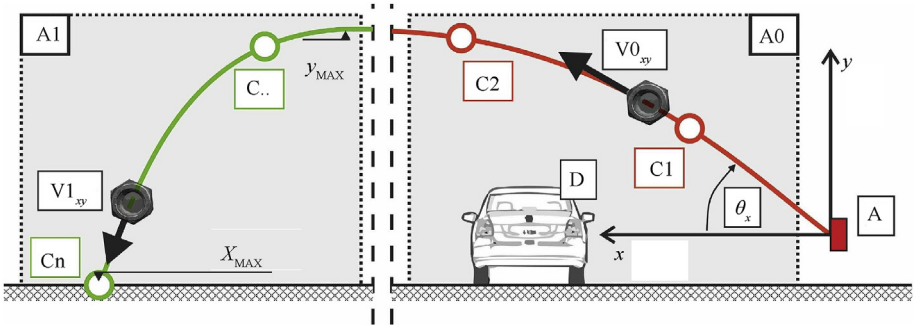

Fig. 5. Range and locations of the primary measurement areas.

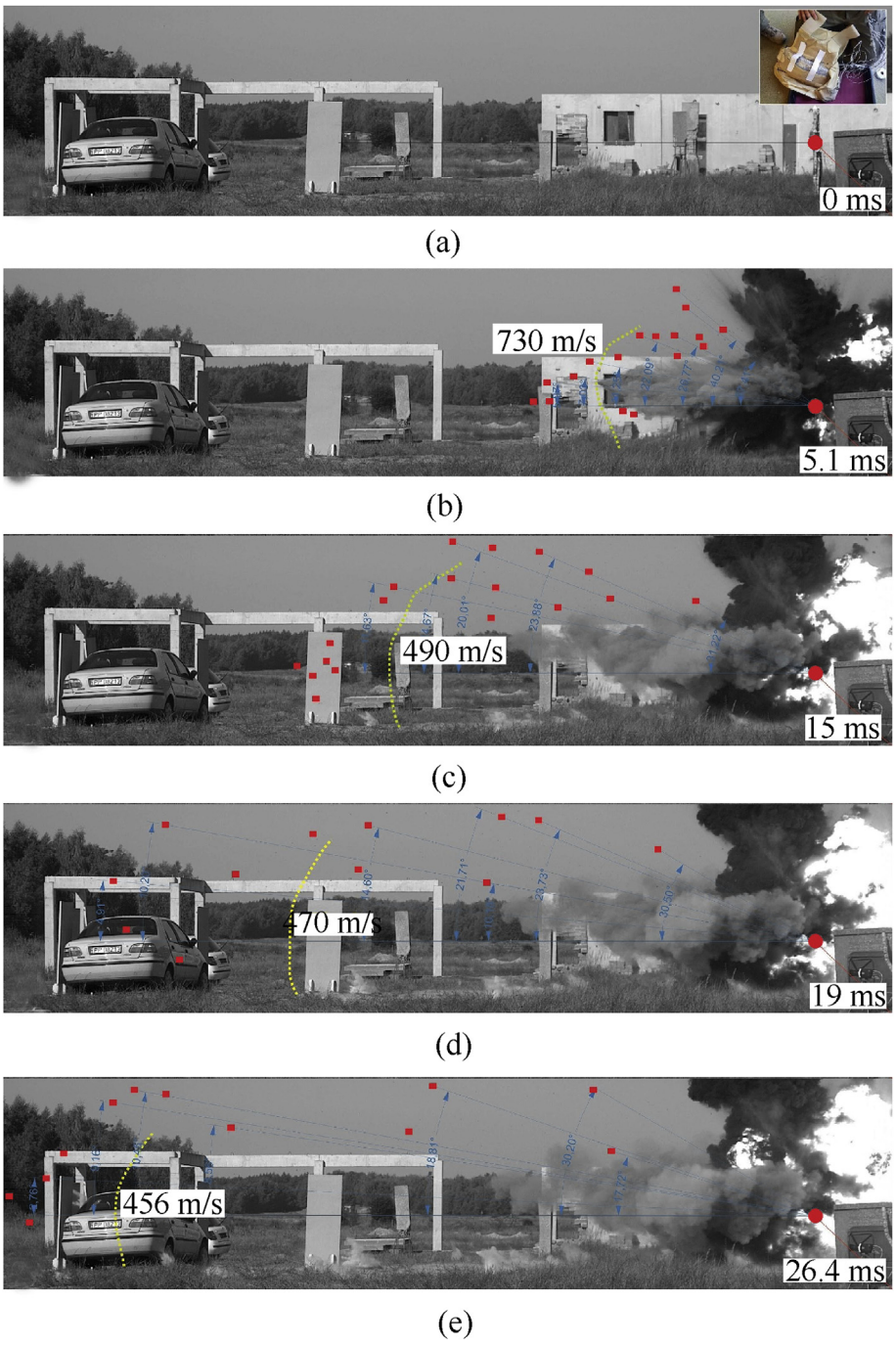

Fig. 6. Sequential time steps from 0 to 26.4 ms after detonation: blast wave movement (yellow dashed lines) and hex nut fragments in flight (red squares).

3. Results and discussion

The explosive field test was conducted in Poland close to the city of Poznan. Fig. 6 shows time-lapse images of the detonation of the PBIED—the blast wave (shock front) and the fragment locations. As documented, the blast wave caused by the detonation overtakes the flying nuts in the first few milliseconds, see Fig. 6(b). The blast wave front is marked with a yellow dashed line. Due to the resolution of the video, the blast wave velocity and how it decreases in time may be observed, compare Fig. 6(b) through Fig. 6(e). The average wave velocity reached 470 m/s, with an estimated incident overpressure value of 15–20 kPa at a distance of 8 m from the PBIED, Fig. 6(d).

Fig. 6 shows the projectile cloud area; for clarity, nuts are marked by red squares. Each nut located within the recording has own location in the experiment based on velocity, trajectory, and time. During the experiment, side boundaries were used, consisting of a rigid box around the vest shown as G in Fig. 1 (a), to catch all projectiles with trajectories greater than $\theta_y = 2.5^\circ$ from a perfect horizontal trajectory or azimuth angle. Thus, it may be stated that the fragments are analysed in two-dimensional plane, i.e. *XY* plane, see Fig. 5.

Acceleration of debris increases in the first few metres, and velocity reaches its maximum magnitude in the next 5–8 m, so the

initial velocity was measured as the average velocity over that 5–8 m. The accuracy of the in-plane distance measurements from the high-speed video is about ±0.05 m, leading to an in-plane accuracy of velocity of about ±0.5%. In addition, if an individual nut's flight trajectory is 2.5° horizontally from the perfect (camera-view plane) trajectory, the out-of-plane error of distance while measuring velocity is approximately 0.01 m (10.8 m−0.8 m × cos 2.5°). Based on the slowest and the fastest fragment measurements, velocity measurements are accurate out-of-plane to less than ±1%. Taking into account both in-plane and out-of-plane directions, the overall velocity measurement error is equal to 1.1%.

The trajectories of 74 nuts were recorded during the field experiment. Two high-speed cameras recorded the velocity and distance measurements from different angles. The primary record was made using a Phantom v711 camera—as used in Sielicki et al. [14,32,34],—located 50 m from the PBIED and perpendicular to the virtual axis A–C, see Figs. 3 and 6. A Phantom Miro320S was used to record the nuts that directly hit the car or the wooden witness obstacles, see camera F, Fig. 3.

During the initial measurement of object trajectories, the number of frames recording these movements is crucial. With a recording speed of 2700 frames per second, Camera F recorded objects on 129 frames due to processing speed limitations. All flying objects were identified in each frame. A similar situation was observed on the primary camera, where the recording speed was 19000 fps, and more than 1100 frames were used. Automatic procedures for monitoring a moving object were applied and implemented in Scilab code with Phantom PCC 3.1 camera control software.

The final data for all 74 measured nuts are presented in Table 2. Note that a negative value of θ_x was obtained if the debris impacted the ground close to the PBIED. Also, some fragments with short landing distances were impossible to measure due to the obscuring effects of the fireball and dust cloud directly after detonation. The peak value recorded was 50° and for instance two pieces of projectile were found only 1.0 m and 2.5 m from the PBIED, thus yielding angle values of −43° and −21°, respectively. Results show that velocity decreased as angle increased—from 500 m/s to 200 m/s.

Experimental data obtained from the field test established boundary conditions for the system's equations of motion. Eq. (1) was used for each fragment to estimate trajectories with particular interest in final resting place and the velocity magnitude just before its contact with the ground, and the kinetic energy was computed. All those data are presented in Table 3. The trajectories computed from Eq. (1) are presented in Fig. 7, where the kinetic energy is shown in colour—black, blue, and grey—for the particular position of the fragment. The energetic criteria are used to assist in the analysis of the harmfulness of the fragments. Three levels of kinetic energy were assigned based on the kinetic energy of the fragment at particular moment. Injury due to the blast wave itself is not analysed in this study; however, this is an important aspect of low mass charge damage, as shown by Gajewski and Sielicki [15,30].

In Fig. 7, fragments drawn in black show the positions of particles with high kinetic energy—greater than 300 J—consistent with typical military bullets (9 mm and greater calibres). As shown by Kerampran et al. [33]; a 9 × 19 mm Parabellum bullet, used widely in military handguns, with a mass of approximately 8 g obtains a velocity of 355 m/s, which results in kinetic energy of approximately 500 J.

Dots in light blue represent positions in which the kinetic energy is moderate—between 20 J and 300 J—which corresponds to the energy of 0.22LR calibre bullets.

The grey dots represent positions with low kinetic energy—below 20 J—which corresponds to pre-charged pneumatic rifle bullet. In Fig. 7, to underline the boundaries between moderate and low kinetic energy, white circles were added.

Fragments with high kinetic energy (black) are highly dangerous to humans. These fragments encountering a human body will cause severe tissue damage, and are most likely pass through the body. Fragments with moderate kinetic energy (light blue) will cause less damage. They are likely to perforate the skin only without going through the body. Fragments with low kinetic energy (grey) are unlikely to perforate skin but will mark the skin, and severe bleeding is possible.

The harmfulness of the fragments accelerated by the PBIED should be assessed based on two criteria. The first criterion is related to close-range harm—up to about 20 m—where the fragments have the greatest kinetic energy, and their trajectory is approximately horizontal (a low or negative vertical trajectory angle θ_x), or their path height is not greater than 2 m (equivalent to about maximum human height). According to this criterion, only the first row of people would be hit with a fragment, but these individuals would experience severe injuries and/or death. People in the second row could be injured if fragments pass through the first row, with or without encountering a first-row body; the second row injuries resulting from fragments that have already impacted others would likely be minor due to fragment energy decrease. In our study, the primary kinetic energy of close range fragments was above 300 J, seeTable 3.

The second safety criterion is related to fragments falling after reaching their maximum heights, as illustrated by the green curve in Fig. 5. The kinetic energy of fragments based on landing distances is shown in Fig. 8. Landing distances were between 120 m and 300 m, with major values greater than 200 m. The kinetic energy of all individual fragments was less than 70 J, with more than 90% below 20 J. Fragments landing at greater distances would have

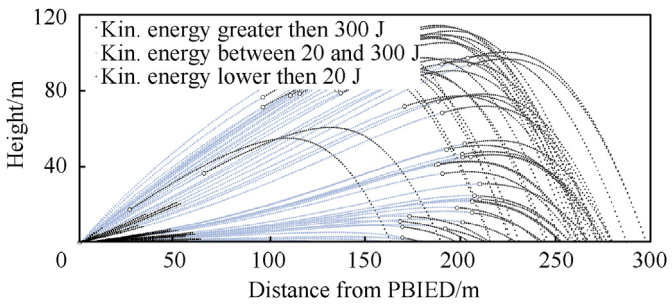

Fig. 7. Computed projectile trajectories – coloured for different kinetic energy.

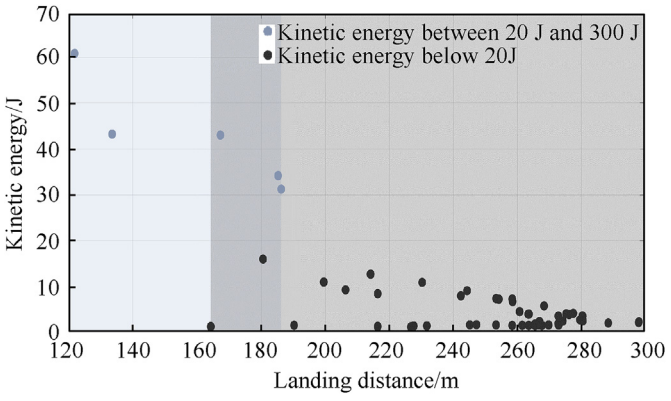

Fig. 8. Kinetic energy of fragments at landing distances.

relatively low harmfulness; more individuals would be affected but injuries sustained would be less severe.

4. Probabilistic data assessment

4.1. Trajectory angle and fragment density

Trajectory angle and fragment density may be treated as a bivariate normal distribution [10,17]; and [18] for vertical (θ_x) and horizontal (θ_y) trajectory angles:

$$p(\theta_x,\ \theta_y) = \frac{1}{2\pi\sigma_x\sigma_y} e^{\left[-0.5\left(\frac{(\theta_x-\mu_x)^2}{\sigma_x^2}+\frac{(\theta_y-\mu_y)^2}{\sigma_y^2}\right)\right]} \tag{2}$$

where μ_x and μ_y are the mean angles of θ_x and θ_y and where σ_x and σ_y are the standard deviations of angles θ_x and θ_y, respectively. If the trajectory angles are equally spread with no bias, then the mean angle is $\mu_x = \mu_y = 0^o$. It might be expected that variability of θ_x and θ_y will be similar. Pope [17] also notes that, for a PBIED, "there is a strong bias for low values of θ_x and θ_y to be selected," suggesting that the variability of angle trajectory will be relatively low.

A statistical analysis of the angle trajectories from 74 fragments (Table 2) reveals $\mu_x = 10.7^\circ$ and $\sigma_x = 18.8^\circ$. The skewness of data towards positive angles may be due to the detonator's location near the bottom of the explosive mass. If the detonator had been placed more centrally, it is more likely that about half the fragments would have a positive angle trajectory, and the other half a negative angle trajectory ($\mu_x \approx 0^{\circ)}$. If the data is limited to include only the 20 negative angles (from -43° to $-0.9^{\circ)}$ and the lowest 20 positive angles' trajectories (from -0.65° to $6.02^{\circ)}$, then $\mu_x = -3.4^\circ$ and $\sigma_x = 8.7^\circ$, and as expected, the mean moves much closer to 0° and variability decreases. The statistics for angle trajectory are clearly variable and highly dependent on the characteristics of the PBIED composition and circumstances of detonation.

Fig. 9 shows that the normal distribution provides a reasonable fit for the data from the 74 fragments described in Table 2. More data is needed to increase confidence in the best probabilistic model fit.

Statistics for the horizontal trajectory angle (θ_y) are not available because the test set-up only allowed fragments to deviate within $\pm 2.5^\circ$. Nonetheless, as noted above, it is expected that variability of θ_x and θ_y will be similar. As a starting point for analysis, two scenarios are considered:

1. PBIED used in current test: $\mu_x = \mu_y = 10.7^\circ$ and $\sigma_x = \sigma_y = 18.8^\circ$
2. Generic IED detonated symmetrically: $\mu_x = \mu_y = 0.0^\circ$ and $\sigma_x = \sigma_y = 18.8^\circ$

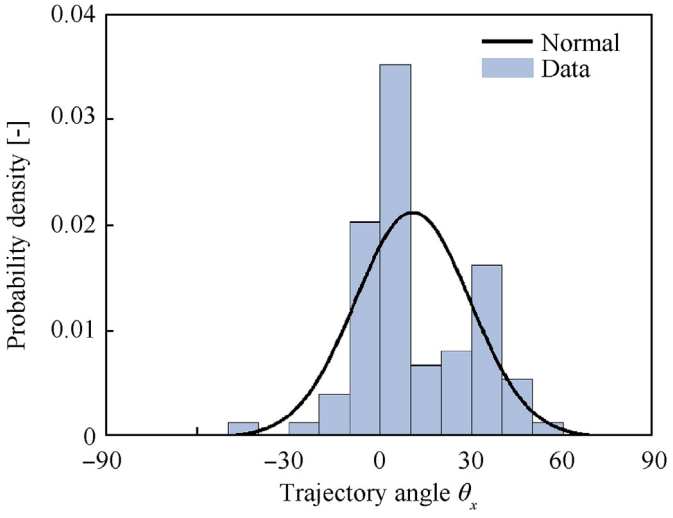

Fig. 9. Histogram of trajectory angles and normal probability distribution.

4.2. Probability of hit

The projected impact area (A_p) is assumed to be rectangular in shape with an aspect ratio (ratio of height to width) of a_{hw}; this allows the height h and width w to be estimated. It is then assumed that the projected area is centred at the same height of the PBIED used in the test (0.9 m), a schematic is shown in Fig. 10. Note that though the fragments have an initial spatial distribution before detonation based on the layout of the hex nuts in a 120 mm × 310 mm layer, for convenience, a "point source" ejection is assumed [17].

The serious injury or fatality zone for a PBIED with a few kilograms of explosive is likely to be no more than about 20–30 m because at that range, the velocity of the fragments will be high and with a relatively close spatial density. At these short distances, it is appropriate to use a line-of-sight approach because, at high speeds, the fragments will travel in approximately a straight line over short distances of <100 m, as shown in Fig. 6(b) and Fig. 7.where R is the distance (range) from the PBIED to the individual (see Fig. 10).

The average number of incapacitating fragments, N, at a distance R hitting the projected area of the exposed person located directly in front of the PBIED is expressed thus:

$$N(R) = n \int_{-\theta_{xi}}^{\theta_{xi}} \int_{-\theta_{yi}}^{\theta_{yi}} p(\theta_x,\ \theta_y)\mathrm{d}\theta_x\,\mathrm{d}\theta_y \tag{3}$$

where n is the total number of fragments ($n = 216$) and the bivariate fragment density distribution $p(\theta_x, \theta_y)$ is given by Eq. (2).

Seven fragments measured at the field test impacted the car D. The projected area of the car is 4.024 m^2, and an aspect ratio of $a_{hw} = 0.33$ is assumed. The dispersion angles from the test are $\mu_x = \mu_y = 10.7^\circ$ and $\sigma_x = \sigma_y = 18.8^\circ$. With these observed parameters and $R = 10.8$ m, Equation (3) yields $N(R) = 7.6$ fragments colliding with the car. If $a_{hw} = 0.25$ or 0.5, then $N(R)$ of the colliding fragments is 7.6 and 7.8, respectively; therefore, the predicted number of colliding fragments is not sensitive to the aspect ratio of the

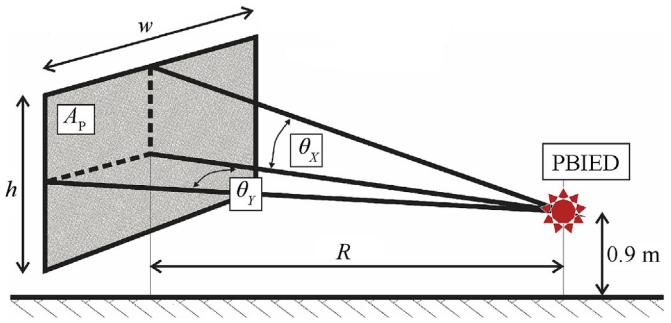

Fig. 10. Schematic illustration of projected impact area, Ap. The trajectory angles needed to affect the projected area are as follows:

$$\theta_{xi} = \pm\tan^{-1}\left(\frac{h/2}{R}\right), \theta_{yi} = \pm\tan^{-1}\left(\frac{w/2}{R}\right),$$

target. A predicted value of $N(R) = 7.6$ fragments compares well with the observed value of seven colliding fragments and provides some validation of the probabilistic modelling of fragment distribution.

The probability of being hit, P_{hit}, by at least one fragment is deduced from the Poisson distribution by the following equation:

$$P_{hit} = 1 - \exp[-N(R)] \quad (4)$$

4.3. Casualty risk assessment

The projected area of an exposed person is $A_p = 0.26\ m^2$ [19]. If it assumed that the aspect ratio for A_p is a height to width of 2, then an exposed person is modelled as a rectangle of height $h = 0.72$ m and width $w = 0.36$ m ($0.36\ m \times 0.72\ m = 0.26\ m^2$).

The density of fragments is not uniformly spread over the surface area of half a hemisphere centred on the exploding device. Fragment density and probability of being hit will be highest if the person stands close to and in front of the PBIED. Those values will reduce as the distance between the person and the IED increases, and the angle from the front of the device increases, i.e. as θ_y increases to 90°. In this case, the average number of incapacitating fragments N at a distance R hitting the projected area of the exposed person is estimated from Eq. (3), and the probability of being hit by a fragment is calculated from Eq. (4) for each horizontal increment (θ_{yi}) until $\theta_y = \pm 90°$. These values are then used to infer the average hit probability for a person anywhere along a circumference with radius R from the PBIED. The probabilities computed according to Eq. (4) are presented in Fig. 11.

4.4. Initial fragment velocity

The statistics of initial fragment velocity, v_o, obtained from launch data from Table 2 are $\mu_v = 405$ m/s and $\sigma_v = 110$ m/s. The variability of initial fragment velocity is high, with a coefficient of variation (COV) of 0.27. Fig. 12 shows the normal, lognormal, Weibull, gamma and Gumbel probability distributions fitted to the experimental data. The comparisons show that the normal distribution provides a good fit to the data, although the lower tail of velocities appears under-predicted. The Kolmogorov–Smirnov test found that all probability models were not rejected at the 5% significance level.

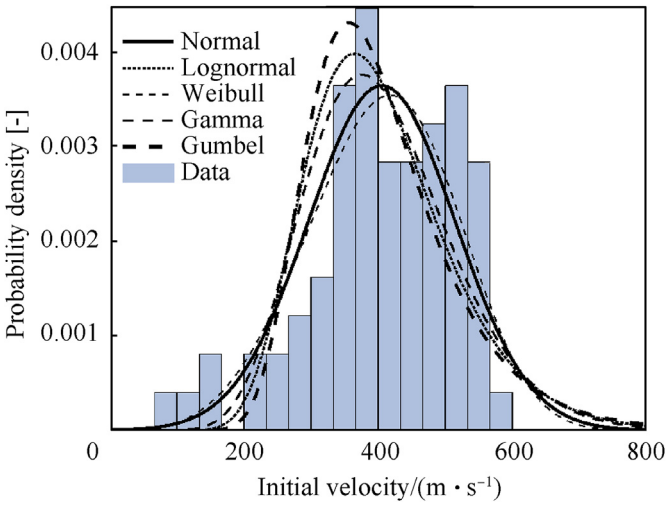

Fig. 12. Comparison of several probabilistic models with data histogram.

Note that the normally distributed random variables used in the present paper are truncated at zero to avoid negative values. Moreover, it should be noted that a probabilistic analysis can also consider non-standard probability distributions (e.g., bi-modal) and it may also allow for truncation of parameter values if there is a physical limit on that value. A benefit of Monte-Carlo simulation is that it can readily incorporate such non-ideal distributions into a probabilistic analysis.

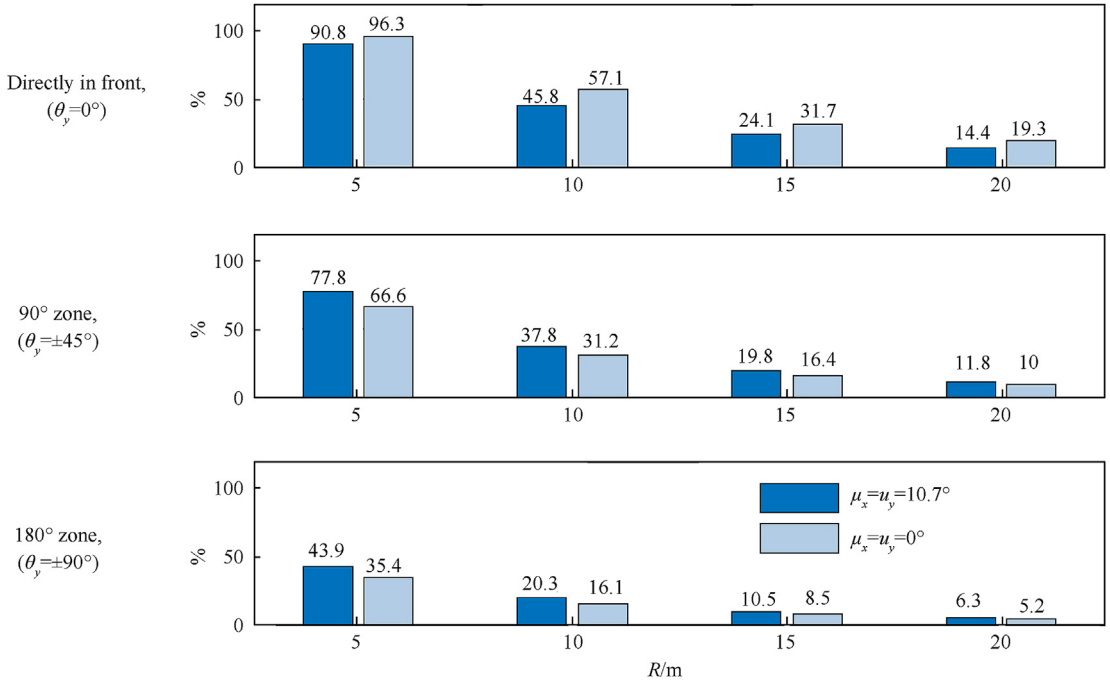

Fig. 11. Probability of being hit by at least one fragment based on location ($\sigma_x = \sigma_y = 18.8°$).

Most research on the initial velocity of fragments is based on cased explosives such as military munitions. Under such circumstances, Gurney equations are used, where the Gurney constant ($\sqrt{2E}$) is given for different types of high explosives. The Gurney constant for plastic explosive C4, which is equivalent to the PE4 used here [20,21] is 2\530 m/s [22]. Gurney equations are provided for cylindrical and spherical charges, thus applicable to most missiles, bombs, and mortars [22]. However, a PBIED typically does not conform to these shape configurations. In our case, the PBIED is attached to stiff supports, which may be model as an infinitely tamped sandwich, see Fig. 1(a). A Gurney analysis for this idealised configuration leads to an initial velocity of the hex nut fragments as follows [23]:

$$v_o = \sqrt{2E}\left(\frac{M}{C}+\frac{1}{3}\right)^{-0.5} \tag{5}$$

where C is the explosive charge mass (kg) and M is the total mass of fragment enhancements (kg). For instance, if $C = 1$ kg and $M = 1$ kg, then initial fragment velocity is equal about 2400 m/s. If the PBIED is model as an open-faced sandwich with no tamping, then the initial fragment velocity is reduced to about 1400 m/s [23]. These calculated model velocities are significantly higher than those observed from the test, where the mean velocity is 405 m/s. This difference can be explained by the layer structure of the PBIED; because the fragments and the explosive were separated by a layer of clay and bulletproof material and not in direct contact, the cross-sectional area of the 216 fragments was smaller than the explosive charge. Pope [17] graphically presents observations regarding "adaptation of Gurney analysis to handle fragment throw-out.", with particular interest in its application to real events.

4.5. Final fragment velocity

The flight of fragments will be affected by air resistance and gravity, leading to the following form of fragment velocity as an approximation to the equations of motion given by Eq. (1) [19]:

$$v = v_o \exp\left(\frac{-kc_d x}{m^{1/3}}\right) \tag{6}$$

where $k = 0.002$ for supersonic velocities ($v_o > 335$ m/s) and 0.0014 for subsonic velocities, v_o is the initial velocity of the fragment, m is the mass of the fragment (kg), x is the distance travelled by the fragment (m), and c_d is the drag coefficient. The drag coefficient is a function of fragment shape, and as previously discussed, the drag coefficients of the nuts are in the range of 0.8–1.5. Hence, in the probabilistic analysis to follow, c_d is taken as a uniform distribution [0.8, 1.5]. If c_d is taken as 1.15 (mean value), then the final fragment velocity at 20 m decreases by approximately 18% and 25% for subsonic and supersonic velocities, respectively.

4.6. Injury models

The injury from penetrating fragments "is of particular interest to the military, and much of the data are from military sources" [19]. The military are more concerned with injuries that will incapacitate but not kill a soldier. However, an incapacitation model has been adapted to estimate fatal and serious injuries by the probit equation:

Table 1
Random variables for casualty risks.

	Mean	Standard Deviation	Distribution
Fragment mass (m)	0.00443 kg	–	Deterministic
Trajectory angles (θ_x, θ_y)	10.7°	18.8°	Normal
	0°	18.8°	Normal
Initial fragment velocity (v_0)	405 m/s	110 m/s	Normal
Drag coefficient(s) (C_{dx}, C_{dy})	1.15	[0.8, 1.5]	Uniform

$$Y = 0.24 + 1.96 \ln\left(v \cdot m^{0.4}\right) \tag{7}$$

where v is the velocity of the fragment (m/s) and m is the mass of the fragment (kg). The probability of serious injury or fatality exceeds 90% if the impact velocity exceeds 190 m/s.

Kinetic energy-based calculations and other probabilistic analyses [19,24] may be used with other injury criteria defined by NATO and the U.S. Department of Defense to predict injuries—for example, incapacitation may occur if the kinetic energy exceeds 79 J (DOD, 2009, [25]. In the instant matter, probabilistic analysis is used to derive the probability of fatal and serious injuries for an individual:

- directly in front of the PBIED ($\theta_x = \theta_y = 0°$)
- anywhere within a 90° zone ($\theta_y = \pm 45°$)
- anywhere within a 180° zone ($\theta_y = \pm 90°$)

at distances from 5 m to 20 m from the PBIED. The random variables are shown in Table 1.

Results from the Monte Carlo simulation are shown in Fig. 13 for 10000 simulation runs. As expected, casualty risks are significantly higher if the person stands directly in front of the PBIED, and the odds reduce if a person is located somewhere else, i.e. $\theta_y > 0°$. Schematics of the location of victims from the 2017 Manchester Arena bombing [26] suggest that most victims were within 10–20 m of the PBIED. The casualty risks in Fig. 13 also show that this range is the zone of high risk, and the risk diminishes beyond 20 m. For example, at 30 m, the casualty risks are about 5% for the 90° zone.

Risks may also be compared with risk acceptance criteria. For example, the UN recommends that, to be considered safe, evacuation distances ensure that the density of hazardous fragments (79 J) is less than 1 per 56 m^2; this is approximately equivalent to a 1% probability of a person being struck by a lethal fragment [22]. If this is the criterion, then an outdoor safe evacuation distance based on a 180° zone is 52 m; this would, however, increase to 69 m if the distance were directly in front of the PBIED. If $\mu_x = \mu_y = 0.0°$ and $\sigma_x = \sigma_y = 18.8°$, the safety distance changes to 46 m and 83 m for the 180° zone and directly in front, respectively. In these cases, a conservative safe evacuation distance for the PBIED considered in the present paper would be approximately 85 m. This is a reasonable estimate given that the United States National Counter Terrorism Center [27] recommends an outdoor safe evacuation distance of 259 m for a 2.3 kg pipe bomb.

4.7. Sensitivity analysis

A sensitivity study is carried out to assess the relative impact of the variability and uncertainty of the model parameters on casualty risks. This was achieved by running the Monte Carlo simulation

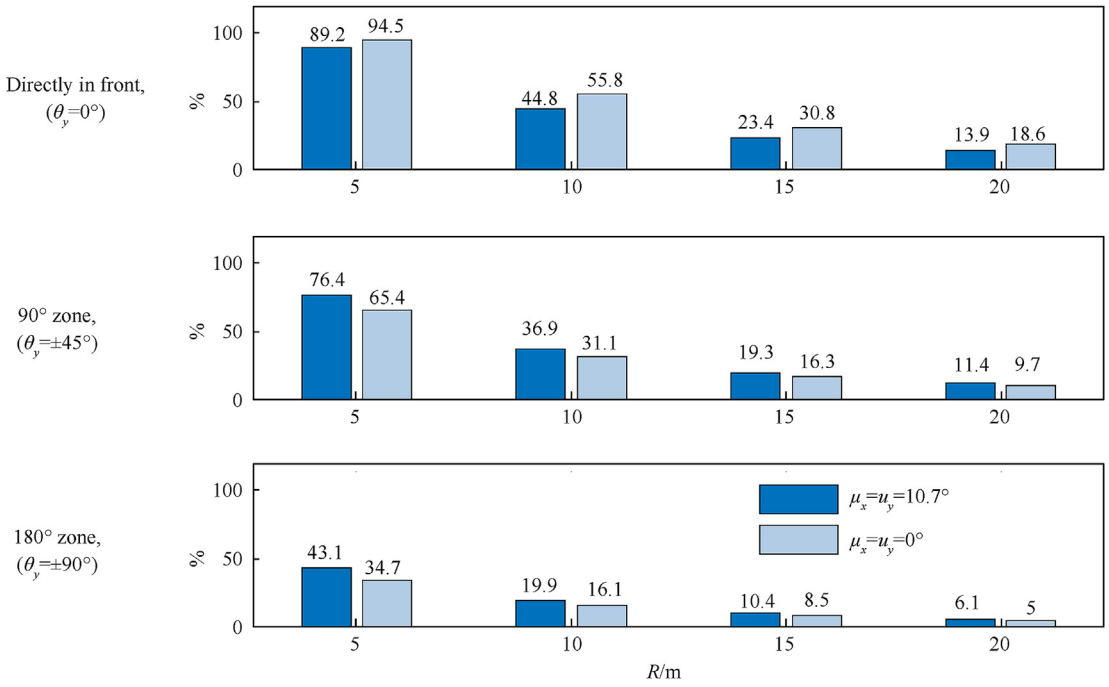

Fig. 13. Probability of fatality or serious injury ($\sigma_x = \sigma_y = 18.8°$).

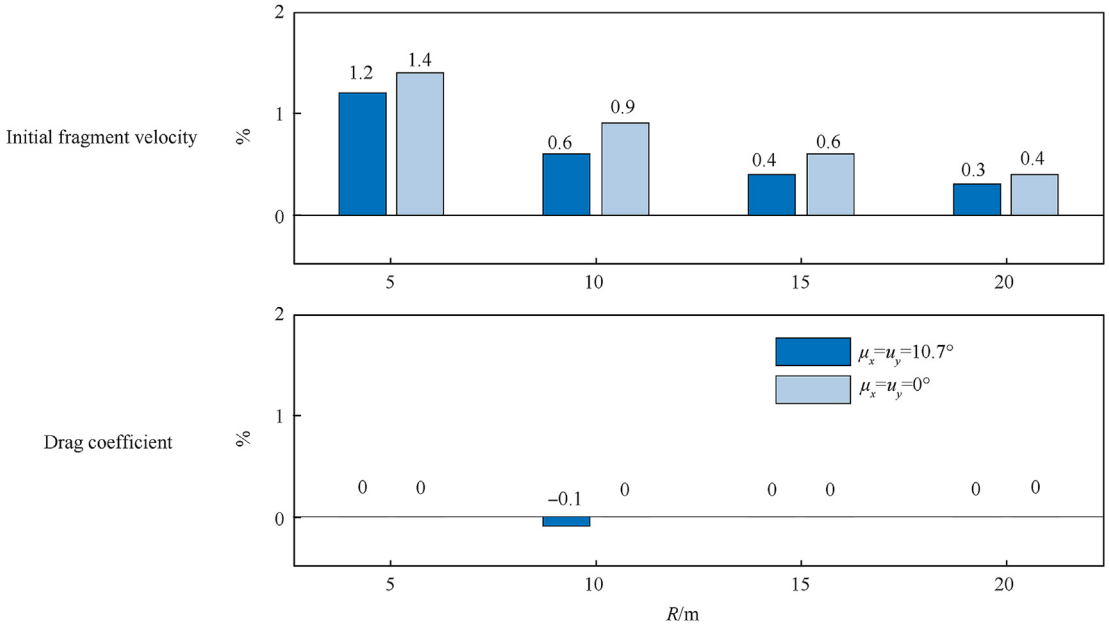

Fig. 14. Change in casualty risks for person directly in front of a PBIED ($\sigma_x = \sigma_y = 18.8°$).

analysis with each parameter in turn modelled deterministically while all other parameters given in Fig. 14 are modelled probabilistically. In Fig. 14, the sensitivity study results are shown as the percentage point-change in casualty risks for a person standing directly in front of a PBIED at a distance of 5 m–20 m. Results are insensitive to drag coefficient variability, and thus, it is concluded that drag coefficient has a negligible influence on the results. Variability of initial fragment velocity changes the casualty risks by less than 1.4% in absolute terms. Clearly, if variability of fragment trajectory angle is omitted from the probabilistic analysis (i.e., $\sigma_x = \sigma_y = 0°$), then casualty risk is near 100% when $\mu_x = \mu_y = 0.0°$.

5. Conclusions

Suicide vest PBIEDs are an important and current topic. An explosive field test for a typical PBIED containing steel fragment (hex nuts) enhancements was used to determine the initial velocities, initial trajectory angles, and kinetic energy of fragments. Those data were then used as boundary conditions to predict the trajectory of suicide vest PBIED fragments according to the classical system of equations of motion. An analysis of fragment harmfulness over various distance from the PBIED detonation. Two crucial aspects for safety were observed: severe harmfulness occurs at close range but with fewer individuals injured, and due to fragments losing velocity, at longer distances, lower harmfulness occurs but more individuals are injured.

Moreover, a probabilistic analysis was then conducted to predict the probability of a person being hit by at least one fragment, a probability of fatality or serious injury, and safe evacuation distances. It was found that fatality risks are 65–95% within 5 m of the PBIED and fall to less than 1% for distances of about 85 m.

Declaration of competing interest

The authors declare that they have no known competing financial interests or personal relationships that could have appeared to influence the work reported in this paper.

Acknowledgements

This work was supported by the Poland National Center for Research and Development, under the grant DOB-BIO10/01/02/2019 within the Defence and Security Programme.

Appendix A

Table 2
Actual measurements of 74 flying nut fragments in the first 0–50 ms after detonation (in descending order of initial incident angle).

Fragment No.	Initial incident angle θ_x[a]/°	Initial velocity v_0[a]/(m·s^{-1})	Initial kinetic energy/J	Fragment No.	Initial incident angle θ_x[a]/°	Initial velocity v_0[a]/(m·s^{-1})	Initial kinetic energy/J
14	−43.36	149	49	24	3.73	535	635
13	−20.65	312	216	39	5.42	441	431
11	−12.78	423	397	31	6.02	501	556
10	−12.19	480	510	32	6.25	486	522
9	−11.18	69	11	38	6.46	427	405
7	−8.42	474	497	40	6.51	428	406
12	−8.37	301	201	33	6.58	481	512
8	−7.96	553	676	36	7.57	483	517
6	−7.89	577	737	37	7.71	446	441
5	−7.82	320	227	47	12.31	456	461
4	−7.00	379	319	48	14.59	447	442
3	−6.62	426	401	49	15.44	416	383
1	−5.38	510	576	50	16.94	379	318
2	−5.22	537	639	51	19.00	524	607
16	−4.31	461	470	52	20.79	518	595
17	−3.67	545	658	53	22.56	460	469
15	−3.28	487	526	55	24.04	364	293
18	−3.24	412	376	54	25.08	388	334
19	−1.48	399	352	56	28.50	357	283
20	−0.90	390	337	73	29.40	153	52
41	0.27	408	369	57	30.33	289	185
42	0.49	383	326	58	32.06	285	180
25	0.52	521	601	59	33.42	313	217
21	0.65	553	677	60	34.21	366	297
22	0.72	534	631	74	35.07	114	29
46	1.55	363	292	61	35.79	381	322
35	1.79	451	450	62	36.41	396	347
30	1.98	492	536	63	37.90	352	275
45	2.19	364	293	64	38.76	363	291
26	2.30	519	597	68	38.80	252	141
44	2.60	359	285	65	39.55	346	265
34	2.74	476	503	66	39.96	385	327
43	2.80	379	318	69	40.36	244	132
23	2.86	539	643	67	41.32	380	320
28	2.87	514	586	70	42.53	218	105
27	2.91	515	589	71	46.65	228	115
29	3.16	519	596	72	50.20	267	158

[a] Values measured at the field test.

Appendix B

Table 3
Prediction of the final fragment range and kinetic energy at ground impact.

Fragment No.	Initial incident angle θ_x[a]/°	Initial velocity v_0[a] /(m·s^{-1})	Maximum horizontal distance /m	Velocity magnitude at ground contact /(m·s^{-1})	Kinetic energy at ground contact /J
14	−43.36	149	1.06	149	49
13	−20.65	312	2.44	312	216
10	−12.19	480	3.70	480	510
11	−12.78	423	4.21	423	397
9	−11.18	69	4.96	69	11
12	−8.37	301	5.94	301	201
8	−7.96	553	7.34	553	676
7	−8.42	474	7.82	474	497
6	−7.89	577	8.09	577	737
4	−7.00	379	9.43	379	319
5	−7.82	320	9.54	320	227
3	−6.62	426	9.96	426	401
2	−5.22	537	11	537	639
16[b]	−4.31	461	12	461	470
1	−5.38	510	13	510	576
17[b]	−3.67	545	14	545	658
15[b]	−3.28	487	16	487	526
18[b]	−3.24	412	16	412	376
19[b]	−1.48	399	35	399	352
20[b]	−0.90	390	57	390	337
41	0.27	408	121	167	62
42	0.49	383	133	141	44
74	35.07	114	163	24	1
25	0.52	521	166	141	44
46	1.55	363	180	86	16
21	0.65	553	184	125	35
22	0.72	534	185	120	32
73	29.40	153	189	27	2
45	2.19	364	199	71	11
44	2.60	359	205	65	9
35	1.79	451	213	77	13
71	46.65	228	215	24	1
70	42.53	218	215	24	1
43	2.80	379	215	62	9
72	50.20	267	226	23	1
69	40.36	244	227	25	1
30	1.98	492	229	71	11
68	38.80	252	231	26	1
34	2.74	476	241	61	8
26	2.30	519	243	65	9
58	32.06	285	244	27	2
57	30.33	289	246	28	2
59	33.42	313	252	27	2
28	2.87	514	252	58	8
27	2.91	515	253	58	7
65	39.55	346	257	26	2
23	2.86	539	257	58	7
29	3.16	519	257	56	7
39	5.42	441	260	46	5
63	37.90	352	261	27	2
38	6.46	427	262	43	4
64	38.76	363	263	26	2
40	6.51	428	263	43	4
56	28.50	357	264	29	2
67	41.32	380	265	26	2
55	24.04	364	266	30	2
60	34.21	366	266	27	2
50	16.94	379	266	33	2
66	39.96	385	267	26	2
24	3.73	535	267	52	6
61	35.79	381	269	27	2
54	25.08	388	272	30	2
37	7.71	446	272	41	4
62	36.41	396	272	27	2
49	15.44	416	273	34	3
32	6.25	486	274	43	4
33	6.58	481	275	42	4
31	6.02	501	276	44	4

Table 3 (*continued*)

Fragment No.	Initial incident angle θ_x[a]/°	Initial velocity v_0[a] /(m·s^{-1})	Maximum horizontal distance /m	Velocity magnitude at ground contact /(m·s^{-1})	Kinetic energy at ground contact /J
47	12.31	456	279	35	3
36	7.57	483	279	41	4
48	14.59	447	279	34	3
53	22.56	460	287	31	2
52	20.79	518	297	32	2
51	19.00	524	297	32	2

[a] Values measured at the field test.
[b] Denotes projectiles for which the initial velocity is roughly measured due to nonideal view.

References

[1] National Academies of Sciences Engineering and Medicine. Reducing the Threat of improvised explosive device attacks by restricting access to explosive precursor chemicals. National Academies Press; 2018. et al.
[2] Williams DS. Enhancing the applicability of blast modelling and advice. Int. J. Protect. Struct. 2015;6(4):701–9. https://doi.org/10.1260/2041-4196.6.4.701. Available at:.
[3] Baranowski P, Małachowski J, Mazurkiewicz Ł. Local blast wave interaction with tire structure. Defence Technol 2020;16(3):520–9. https://doi.org/10.1016/j.dt.2019.07.021. Available at:.
[4] Al-Rifaie H, Sumelka W. Improving the blast resistance of large steel gates—numerical study. Materials 2020;13(9). https://doi.org/10.3390/ma13092121.
[5] Yeh D, Schecter W. Primary blast injuries-an updated concise review. World J Surg 2012;36(5):966–72.
[6] Mathews ZR, Koyfman A. Blast injuries. J Emerg Med 2015;49(4):573–87.
[7] Mazurkiewicz Ł., Małachowski J, Baranowski P. Optimization of protective panel for critical supporting elements. Compos Struct 2015;134(15):493–505. https://doi.org/10.1016/j.compstruct.2015.08.069.
[8] Stewart MG, Mueller J. Terrorism risks, chasing ghosts, and infrastructure resilience. Sustain Resilient Infrastruct 2020;5(1–2):78–89.
[9] Yokohama H, et al. Vehicle borne improvised explosive device (VBIED) characterisation and estimation of its effects in terms of human injury. Int. J. Protect. Struct. 2015;6(4):607–27. https://doi.org/10.1260/2041-4196.6.4.607. Available at:.
[10] DDESB. Approved methods and algorithms for DoD risk-based explosives siting. Alexandria, VA: Department of Defense Explosives Safety Board (DDESB); 2009. 21 July 20090.
[11] Pachman J, et al. Study of TATP: blast characteristics and TNT equivalency of small charges. Shock Waves 2014;24:439–45. https://doi.org/10.1007/s00193-014-0497-4.
[12] Moxnes JF, Frøyland Ø, Øye IJ, Brate TI, Friis E, Ødegårdstuen G, Risdal TH. Projected area and drag coefficient of high velocity irregular fragments that rotate or tumble. Defence Technol 2017;13(4):269–80.
[13] Kljuno E, Catovic A. Estimation of projected surface area of irregularly shaped fragments. Defence Technol 2019;15(2):198–209. https://doi.org/10.1016/j.dt.2019.01.007. Available at:.
[14] Sielicki PW, Sumelka W, Łodygowski T. Close range explosive loading on steel column in the framework of anisotropic viscoplasticity. Metals 2019;9(454). https://doi.org/10.3390/met9040454.
[15] Gajewski T, Sielicki PW. Experimental study of blast loading behind a building corner. Shock Waves 2020;30:385–94.
[17] Pope DJ. The development of a quick-running prediction tool for the assessment of human injury owing to terrorist attack within crowded metropolitan environments. Phil Trans Biol Sci 2011;366(1562):127–43. https://doi.org/10.1098/rstb.2010.0261. Available at:.
[18] van der Voort M, Weerheijm J. A statistical description of explosion produced debris dispersion. Int J Impact Eng 2013;59:29–37.
[19] Mannan S. Lees' loss prevention in the process industries. Amsterdam: Butterworth-Heinemann; 2012.
[20] Rigby SE, Sielicki PW. An investigation of TNT equivalence of hemispherical PE4 charges. Eng Trans 2014;4:423–35.
[21] Bogosian D, Yokota M, Rigby SE. TNT equivalence of C-4 and PE4: a review of traditional sources and recent data. In: Proceedings of the 24th military aspects of blast and shock. Halifax: Nova Scotia; 2016. Canada 2016.
[22] UN. *Formulae for ammunition management*, international ammunition technical guideline, IATG – 01.80. United Nations Office for Disarmrment Affairs; 2015.
[23] Kennedy JE. The Gurney model for explosive output for driving metal. In: Zukas JA, Walters WP, editors. Explosive effects and applications. New York: Springer; 1998. p. 221–57.
[24] UFC 3-340-02. Structures to resist the effects of accidental explosions, unified facilities criteria (UFC). Washington, D.C: US Department of Defense; 2014.
[25] AASTP-1. Manual of NATO safety principles for the storage of military ammunition and explosives. Allied Ammunition Storage and Transport Publication (AASTP), Edition B; 2015., Version 1.
[26] BBC. Manchester attacks: minute's silence at opening of inquests. BBC News; 2017. 9 June 2017, https://www.bbc.com/news/uk-england-manchester-40217591. [Accessed 2 August 2019].
[27] NCTC. US National counter terrorism center (NCTC) bomb Threat stand-off distances. 2005. https://www.dni.gov/files/NCTC/documents/features_documents/2006_calendar_bomb_stand_chart.pdf.
[30] Sielicki PW, Gajewski T. Numerical assessment of the human body response to a ground-level explosion. Comput Methods Biomech Biomed Eng 2019;22(2):180–205.
[32] Sielicki PW, Pludra A, Przybylski M. Experimental measurement of the bullet trajectory after perforation of a chambered window. Int J Appl Glass Sci 2019;10(4):441–8. https://doi.org/10.1111/IJAG.13478.
[33] Kerampran C, Gajewski T, Sielicki PW. Temperature Measurement of a Bullet in Flight. Sensors 2020;20(24). https://doi.org/10.3390/s20247016.
[34] Ślosarczyk A, Szulc D. Concrete slab fragmentation after bullet impact: An experimental study. Int J Prot Struct 2019. https://doi.org/10.1177/2041419619854764.